RICHARD J. PHILLIPS

Microchannel Heat Sinks

Microchannel heat sinks can be used in a wide variety of applications, including microelectronics, diode laser arrays, and high-energy-laser mirrors. Heat sinks that can be used to cool diode laser arrays have been fabricated in indium phosphide (InP) with a thermal resistance as low as $0.072°C/(W/cm^2)$, which allows these devices to dissipate loads in excess of $1,000 \ W/cm^2$. This thermal resistance is nearly two orders of magnitude lower than that achieved by the methods presently used in the microelectronics industry. A heat-sink thermal- and fluid-performance model is presented; microchannel fabrication techniques are described for InP and aluminum.

The contradictory requirements of high heat dissipation and low temperature rise are commonly demanded for a wide variety of applications. (For a description of some of the potential uses for microchannel heat sinks, see Box, "Applications.") High-energy-laser mirrors, surface-emitting laser diode arrays, and high-speed microelectronic devices, for example, can dissipate 10 to $1,000 \ W/cm^2$, yet temperature rises generally must not exceed 100°C. The unique construction of microchannel heat sinks enables these elements to bring a heat source and a heat sink into very close thermal proximity, thus minimizing thermal resistance.

A microchannel heat sink consists of very small channels and fins in a parallel arrangement (Fig. 1). The heat sink is very close to the device that requires cooling; conduction transfers heat from the active device to the heat sink. Heat is then transferred from the heat sink to the outside world by passing a coolant, usually a liquid, through the channels.

The distinguishing feature of microchannel heat sinks is the size of their cooling channels. The same microfabrication techniques that are used for the fabrication of electronic devices can be used to make heat sinks [1-4]. These techniques permit reliable fabrication of high-precision channels with channel widths, W_c, and fin widths, W_w, as small as 50 μm and channel heights, b, as great as several hundred microns. When liquids like water are forced through these channels under pressures on the order of 10 psi, heat transfer rates can rival boiling heat transfer. (To withstand the coolant

pressure, the substrate must have a thickness, t, on the order of 100 μm).

CONVECTIVE FLUID FRICTION AND HEAT TRANSFER

As with other heat-dissipation analyses, thermal and fluid performance for microchannel heat sinks can be modeled with Reynolds numbers, apparent friction factors, Nusselt numbers, and parameters that describe the thermal and fluid performance of the coolant. The thermal performance depends, in part, on whether the coolant flow is laminar or turbulent.

As coolant enters a channel (Fig. 2), a boundary layer develops within the coolant. This boundary layer separates the uniform-velocity core from the stationary coolant at the wall (the "no-slip" boundary condition). The boundary layers will increase in thickness as the coolant flows through the channel, until the velocity profile achieves a "fully developed" profile, which does not change with downstream distance. The flow upstream from that point is said to be "developing"; the flow downstream is "fully developed."

The Reynolds number, Re, which is the ratio of inertial to viscous fluid forces, can be used to estimate the transition between laminar and turbulent flow:

$$Re = \frac{V \, De}{\nu_f}$$

where V is the average coolant velocity in the channel, De is the equivalent diameter of the

Applications

Microchannel heat sinks offer solutions to thermal dissipation problems for many existing and developing applications. As shown in the Fig., heat dissipation rates in computer modules can reach levels that equal those encountered by space vehicles upon reentry into the earth's atmosphere [18]. But unlike reentry vehicles, the maximum surface temperature of the ICs in computer modules usually must be less than 100°C. In contrast, reentry vehicles are designed to withstand temperatures of more than 1,000°C.

Because high-energy-laser mirrors typically absorb about 0.1% of incident laser energy, they can experience heating rates of 10 to 100 W/cm². In spite of this high thermal flux, the temperature variation of these mirrors must be minimal. Distortion of as little as 250 Å can seriously degrade the optical performance of a high-energy-laser mirror.

Arrays of surface-emitting GaInAsP/InP diode lasers are being developed as laser pumping sources, optical interconnects for ICs, and as two-dimensional communication-switching devices. These arrays require high-capacity, high-efficiency heat sinks.

The Table lists thermal parameters for some state-of-the-art computer modules. The highest heat dissipation demonstrated to date is 40 W/cm² for a single-chip module. Multichip modules have somewhat lower heat dissipation figures. When averaged across an entire multichip module, heat dissipation is generally less than 3 W/cm². Use of microchannel heat sinks could accommodate more than 1,000 W/cm².

Prototypes of microchannel heat sinks for commercial applications are under development. Devices may be marketed by 1990 — less than ten years after the first development of the technology.
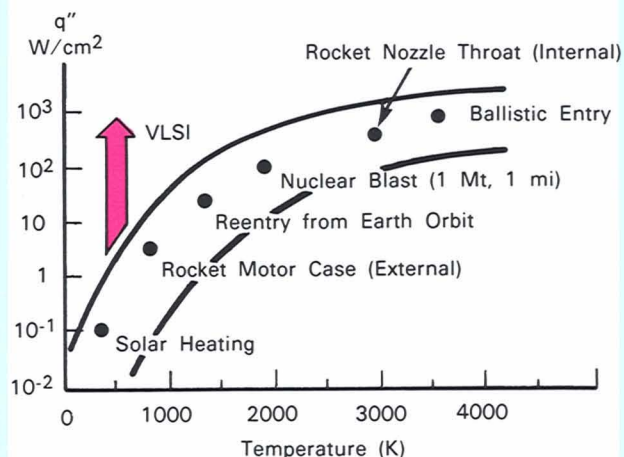
Very large scale integrated circuits dissipate on the order of 10 W/cm². Within the next decade, some chips will dissipate 100 W/cm² — as much heat as a nuclear blast [18].

Thermal Parameters for Computer Modules[a]

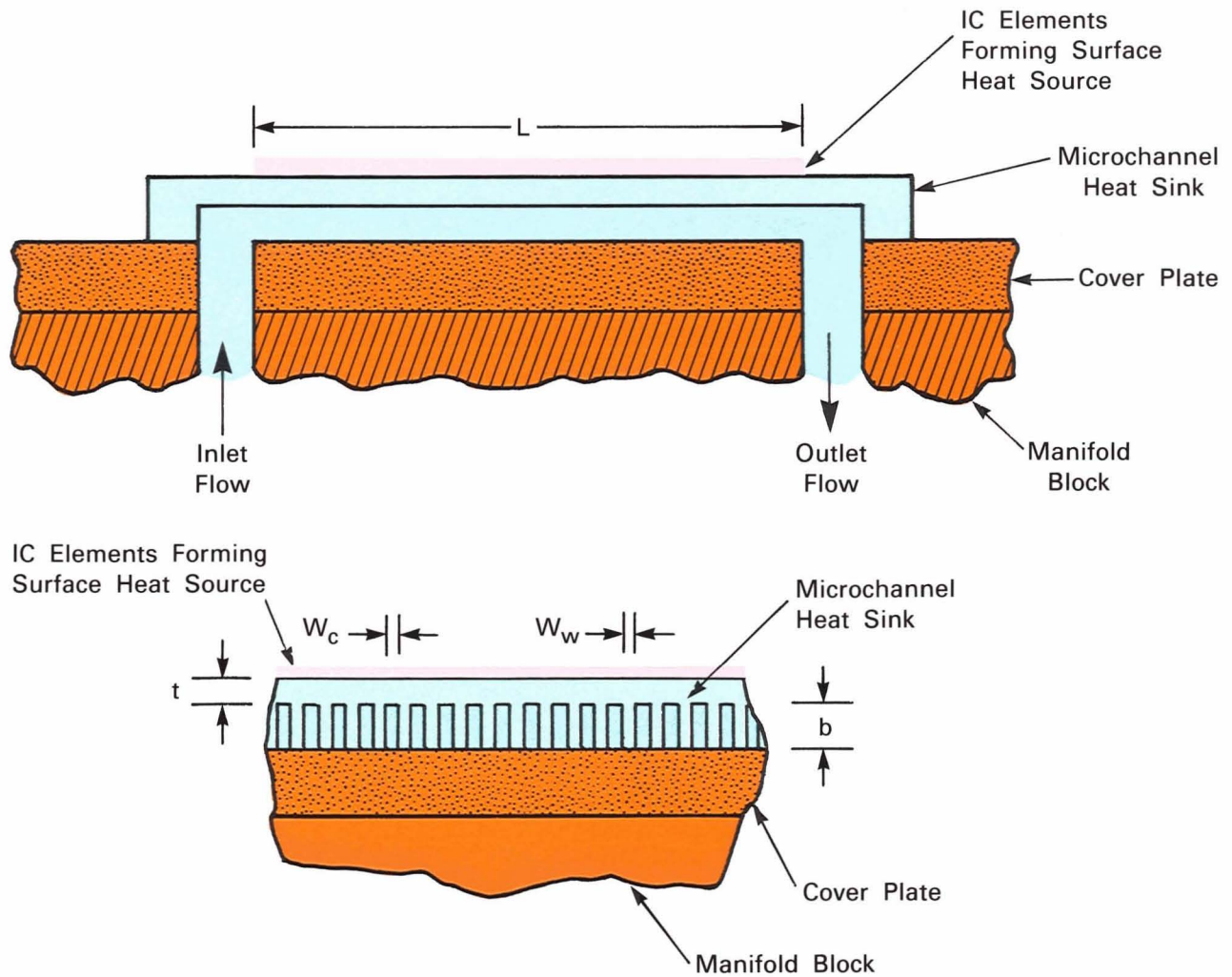| Technology	Maximum Chip q'' (W)	Average Module q'' (W)	R_{tot} (°C/W)
Single Chip			
Hp Finstrate	10.1	—	<8.7
Hitachi S-810	13.1	—	7.0
Burroughs PGA	24.3	—	12
Motorola MCA-2	24.5	—	3.3
Sperry Compact HX	40	—	4.9
Multichip Module			
Mitsubishi HTCM	6.25	0.83	7.3
NEC SX LCM	>8.4	1.6	5
Hitachi RAM	13.1	0.8	34.7
IBM 4381	17.0	2.2	17.0
IBM 3090 TCM	29.8	2.2	8.7

[a]See Ref. [18]

Fig. 1 — *These views of a microchannel heat sink include the side view, which shows the longitudinal coolant flow through a heat sink with channel length, L. The bottom, "end-on" view shows the channel width, W_c, fin width, W_w, channel height, b, and substrate thickness, t.*
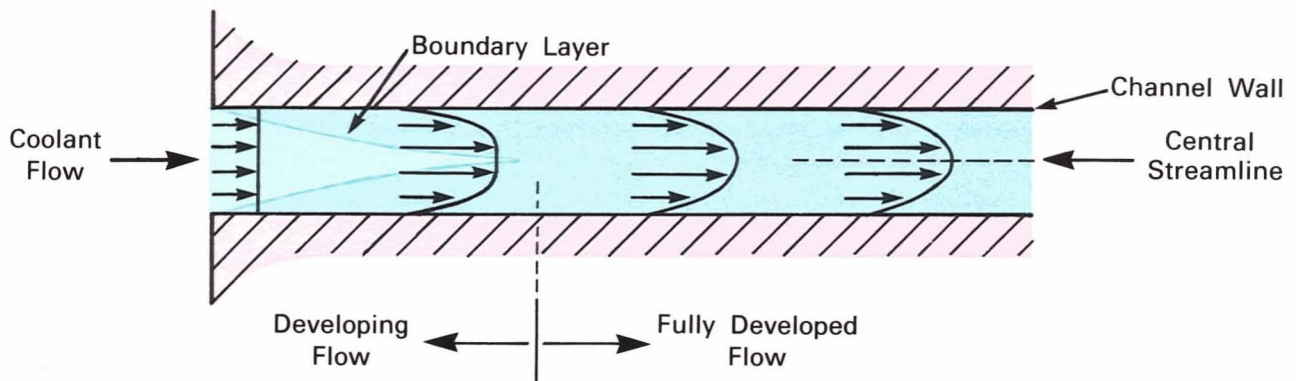

Fig. 2 — *As coolant flows through a channel, the flow pattern changes from "developing" to "fully developed" flow. The distinctive feature of developing flow is a change in the velocity profile of the coolant. The profile vectors change in the region of developing flow, but remain constant in the fully developed region.*

channel [here De = $\frac{4}{\wedge}$ b $W_c/(2W_c + 2b)$], and ν_f is the kinematic viscosity of the coolant. Channel flow is usually considered to change from laminar to turbulent flow at Re $\approx$ 2,300.

The thermal and fluid performance characteristics of a coolant depend on both the flow regime and on whether the flow is fully developed. In general, the rate of heat transfer increases as the coolant velocity increases. But as the coolant velocity increases, the coolant pressure-drop also increases, and greater pumping power is necessary.

The coolant experiences a pressure drop ΔP of

$$\Delta P = 4f_{app} \left(\frac{L}{De}\right) \left(\frac{\rho_f V^2}{2\,g_c}\right)$$

where f_{app} is the apparent friction factor, L is the channel length, ρ_f is the coolant density, and g_c is a units constant. The low-Reynold's-number, turbulent-flow apparent friction fac-
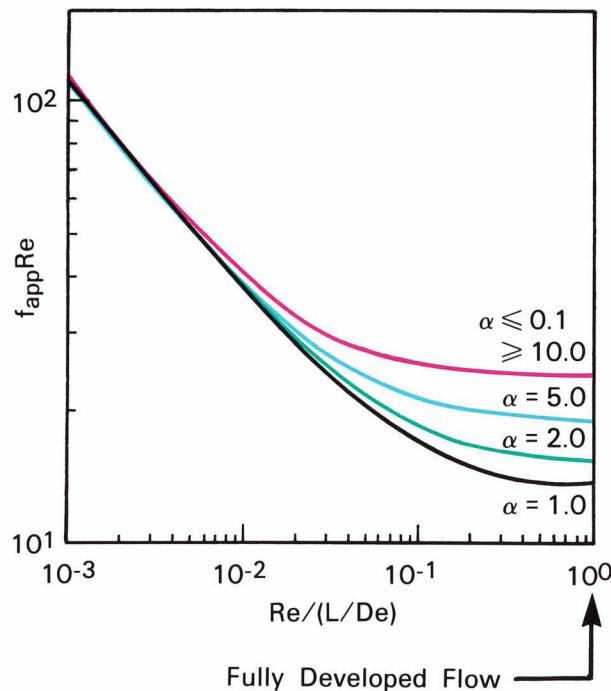

Fig. 3 — Laminar-flow apparent friction factor varies with channel aspect ratio and Reynolds number. A channel aspect ratio of 1:1 (channel width equals channel height) provides the lowest f_{app} Re product.

Table 1 — Approximate Values of Convection Heat Transfer Coefficients [7]

Mode	h (W/m²°C)
Free convection, air	5-25
Forced convection, air	10-500
Forced convection, water	100-15,000
Pool boiling, water	2,500-35,000
Flow boiling, water	5,000-100,000

tor [5] can be expressed as

$$f_{app} = A\,(Re^*)^B$$

where

$$A = 0.0929 + \frac{1.01612}{L/De}, \quad B = -0.2680 - \frac{0.31930}{L/De},$$

and Re^* is based on the "laminar equivalent diameter" of a rectangular channel $[(2/3) + (11/24\,\alpha) \times (2 - 1/\alpha)]$ De . In Fig. 3, the laminar-flow apparent friction factor is plotted as a function of channel aspect ratio ($\alpha = b/W_c$).

The rate of heat transfer per unit area, q″, from the channel walls to the coolant is proportional to the heat transfer coefficient, h:

$$q'' = h\,\Delta T$$

where ΔT is the temperature difference between the channel wall and the coolant. The heat transfer coefficient is usually expressed in the form of the dimensionless Nusselt number, Nu:

$$Nu = \frac{h\,De}{k_f} \qquad (1)$$

where k_f is the thermal conductivity of the coolant. The Nusselt number for turbulent flow is [6]

$$Nu = 0.012\left[1.0 + \left(\frac{De}{x}\right)^{2/3}\right] (Re^{0.87} - 280)\,Pr^{0.4} \qquad (2)$$

where x is the distance from the channel entrance and Pr is the Prandtl number of the coolant (the ratio of hydrodynamic to thermal diffusivities of the coolant). The Nusselt number for laminar flow with several channel aspect ratios is illustrated in Fig. 4.

As Fig. 4 shows, a microchannel heat sink with an aspect ratio of 4 can have a fully developed Nusselt number of 5.35. Using Nu = 5.35, k_f = 0.6 W/m-°C (liquid water), and assuming a channel equivalent diameter (De) of 100 μm, Eq. 1 gives a heat transfer coefficient of about 32,000 W/m²-°C.

Table 1 compares the approximate range of heat transfer coefficients commonly found in other modes of heat transfer [7]. The rate of heat transfer from microchannel heat sinks is orders of magnitude higher than for forced-air convection, and is comparable to that of boiling heat transfer. But because impulsive expansions are associated with boiling heat transfer, this method can reduce the reliability of integrated circuits (ICs).

THERMAL RESISTANCE MODEL

A close look at the thermal model of a heat sink reveals the key to the microchannel heat sink's performance advantage. The thermal performance of a heat sink is often specified in terms of its total thermal resistance. Several common assumptions are used to construct a thermal-resistance model. For example, it is assumed that the coolant flow is steady and
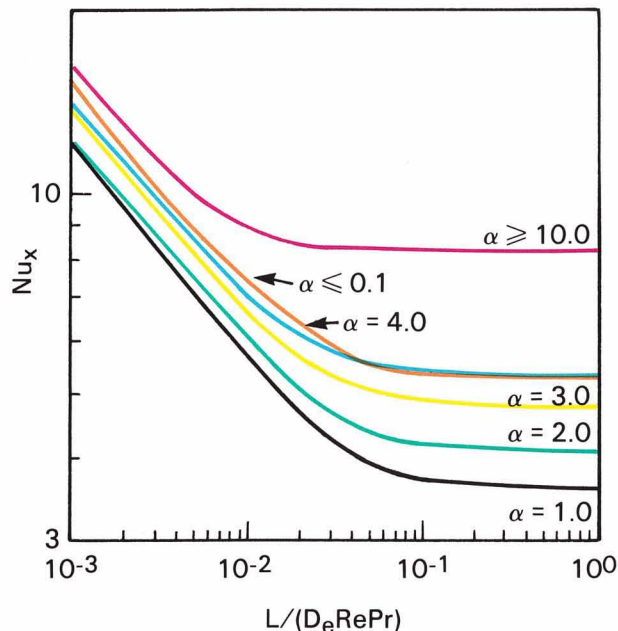

Fig. 4 — *Deeper channels increase the Nusselt number.*

incompressible, that the surface heating is spatially and temporally constant, that the temperature gradient through the fin thickness is small compared with that along the fin height, and that the fin tip is insulated (no heat transfer from the cover plate). Conduction of heat in the streamwise direction in the fin and the coolant is ignored. It is also assumed that the coolant temperature and the heat transfer coefficient are uniform over the entire channel surface at any given distance from the channel entrance.

Based on a single channel and an adjacent fin, the total thermal resistance, R''_{tot}, is

$$R''_{tot} = L (W_w + W_c) \left(\frac{\Delta T_{surf}}{Q} \right) = \frac{\Delta T_{surf}}{q''}$$

where ΔT_{surf} is the peak surface-temperature rise above the inlet coolant temperature (ignoring viscous dissipation heating), Q is the total heating rate over the channel and fin pair, and q'' is the uniform surface heating rate per unit area.

The total thermal resistance can be divided into several components. Figure 5 identifies six of these components. If many discrete heat sources are used, the thermal-spreading (heat dispersion) resistance, R''_{spread}, distributes the heat flow until the heat flow just below the surface of a discrete heat source (such as an IC) is uniform. This thermal-spreading resistance is

$$R''_{spread} = \frac{L (W_w + W_c)}{c \, k_w \, a}$$

where c is a constant that depends on the shape of each heat source (*eg*, c = 4 for a square heat source [8]), k_w is the thermal conductivity of the material, and a is the characteristic dimension of the heat source shape.

Conduction through the solid material between the heat-source surface and the channel-base-fin-base plane adds another component to the thermal resistance. This resistance, R''_{solid}, is

$$R''_{solid} = \left(\frac{t}{k_w} \right)_1 + \left(\frac{t}{k_w} \right)_2$$

where t is the thickness of each solid layer, and k_w is the thermal conductivity of the material.
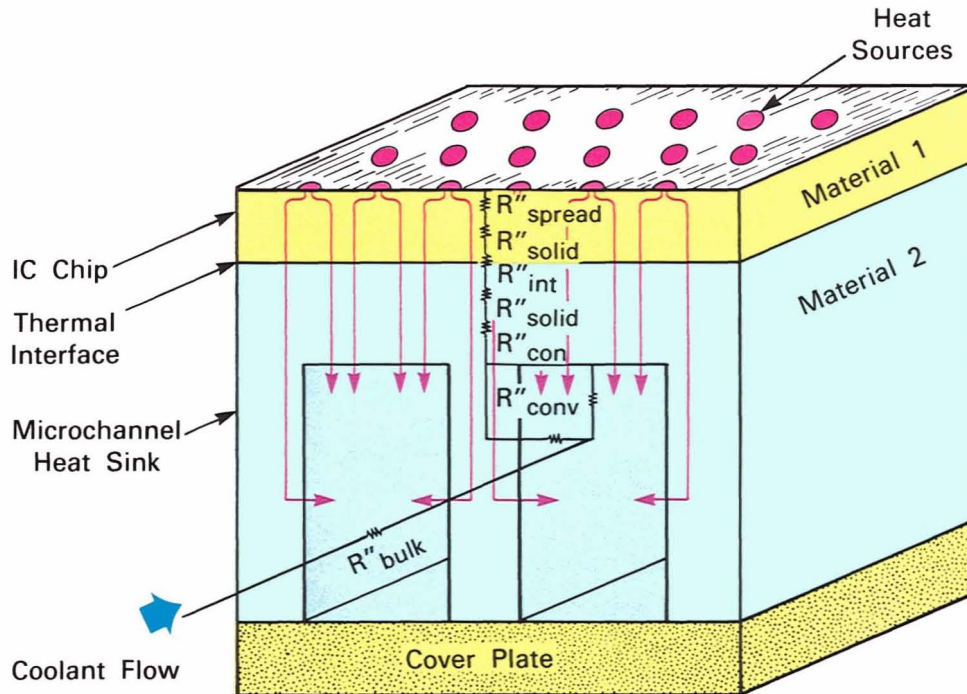
Fig. 5 — Thermal resistance components.

The interface between the heat source and the heat sink gives rise to the interface thermal resistance, R''_{int}. A microchannel heat sink can be manufactured as an integral part of an IC, which eliminates this component of thermal resistance. However, if a heat sink is built separately and then attached to a heat source (a "cold plate" arrangement) then the value of R''_{int} depends upon the attachment method. Various thermal interfaces, such as solder and epoxy bonding, thermal grease, and gas layers are in common use. A newly developed method, the microcapillary thermal interface, provides very low thermal resistance [4,9]. (For more details, see Box, "Thermal Interface Techniques.")

Fins transfer more heat than the fin-base surface could if it were directly exposed to the coolant. The heat flow is therefore funneled into the base of the fin. The thermal resistance due to constriction, R''_{con}, is [10]

$$R''_{con} = \frac{(W_w + W_c)}{\pi k_w} \ln \frac{1}{\sin[\pi W_w/(2W_w + 2W_c)]} \quad .$$

This equation assumes that all of the heat is conducted through the fin before being convected to the coolant. In reality, some heat is convected from the channel base, thereby making the constriction thermal resistance somewhat smaller than predicted. This difference is small and is ignored for simplicity.

A convection thermal resistance, R''_{conv}, is associated with heat conduction through the fin and convection from the fin and channel base surfaces. The value of this resistance component is

$$R''_{conv} = \frac{(W_w + W_c)}{h\,W_c + 2\,h\,b\,\eta_f} \tag{3}$$

Thermal Interface Techniques

The thermal resistance between a heat source and a heat sink can be lowered in several ways. Bonding methods (epoxy, solder, etc.) form a solid interface. A solid interface, however, is subject to mechanical stress due to the differences between the coefficients of thermal expansion of a heat sink and a heat source. And a solid bond can have gas voids, which act as thermal insulators. Furthermore, a solid bond can be formed only once — a heat sink cannot be easily removed without damaging itself or the heat source.

Gas-layer interfaces, such as He, are difficult to implement because they require a microscopic interface gap between optically flat dust-free surfaces. Liquid-layer interfaces, such as thermal grease, often require large compressive loads to keep the interface gap small.

The microcapillary interface, developed at Stanford University, provides a low-resistance interface that has none of the above problems [4,9]. As shown in the Fig., this interface uses reentrant channels that are partially filled with a high-surface-tension liquid. The surface tension develops a strong attractive (suction) force between the two surfaces, resulting in an interfacial gap that is typically less than 0.7 μm. The interface is reusable; the heat sink and the heat source can be separated without damage to either device. Because the interface is a liquid, differences in thermal coefficients of expansion do not cause problems. Moreover, the close spacing of the heat source and heat sink does not require optically flat surfaces or large compressive loads. Thermal resistance as low as 0.02°C/(W/cm^2) have been measured for this type of interface.
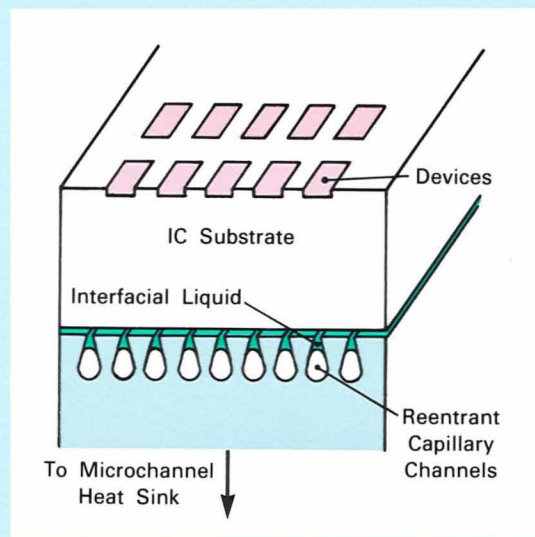
This microcapillary interface features a thin gap with low thermal resistance.

where η_f is the fin efficiency:

$$\eta_f = \frac{\tanh{(mb)}}{mb} \,, \; m = \left(\frac{2h}{k_w W_w}\right)^{0.5} .$$

The first term in the denominator of Eq. 3 represents convection from the channel base; the second term represents convection from the fin.

The final thermal resistance component is associated with the bulk temperature rise of a liquid coolant from the channel entrance. This temperature rise is caused by absorption of heat from fin and channel base surfaces. The coolant bulk temperature rise thermal resistance, R''_{bulk}, is

$$R''_{bulk} = \frac{x(W_w + W_c)}{\rho_f \, C_{pf} \, b \, W_c \, V}$$

where C_{pf} is the coolant specific heat.

One phenomenon causes a temperature rise independent of the heating rate, so it cannot be formulated as a thermal resistance. This is the coolant temperature rise due to the conversion of mechanical energy (fluid pressure) into thermal energy (fluid temperature rise), ΔT_{visc}:

$$\Delta T_{visc} = \frac{\Delta P}{\rho_f \, C_{pf} \, J}$$

where J is the mechanical equivalent of heat (1.0 N-m/J).

Combining the total thermal resistance components, the total temperature rise, ΔT_{tot}, of the heat source surface, including viscous dissipation effects is

$$\Delta T_{tot} = R''_{tot}\, q'' + \Delta T_{visc} \tag{4}$$

where

$$R''_{tot} = R''_{spread} + R''_{solid} + R''_{int} + R''_{con}$$
$$+ R''_{conv} + R''_{bulk} \quad .$$

Figure 6 shows a typical surface temperature distribution in the streamwise direction of the coolant. The surface temperature increases with distance from the channel entrance because the coolant temperature rises and because the heat transfer coefficient decreases with distance from the channel entrance. (Nu decreases with increasing x — see Eq. 2 and Fig. 3.) If the microchannel heat sink is longer than the surface heat source, some heat is conducted laterally from the heat source [5], as

shown in Fig. 7. The dotted curve of Fig. 6 shows the coolant temperature; the dashed curve shows the surface temperature.

PERFORMANCE PREDICTIONS

Based on the thermal-resistance model summarized in Eq. 4, a computer program was written. This program predicts the thermal and fluid performance of microchannel heat sinks. A complete program listing appears in Ref. 5. The program has been used to compute the thermal and fluid performance for a wide variety of coolant flow-rate constraints and heat-sink designs. It permits variable property effects in both the coolant and in the heat-sink material.

The coolant is assumed to be a liquid, so compressibility effects in the coolant are not included in the computations. Furthermore, R''_{spread} and R''_{int} are omitted from the calculations. R''_{spread} usually is small and varies considerably with geometry; R''_{int} varies considerably with the type of interface used.
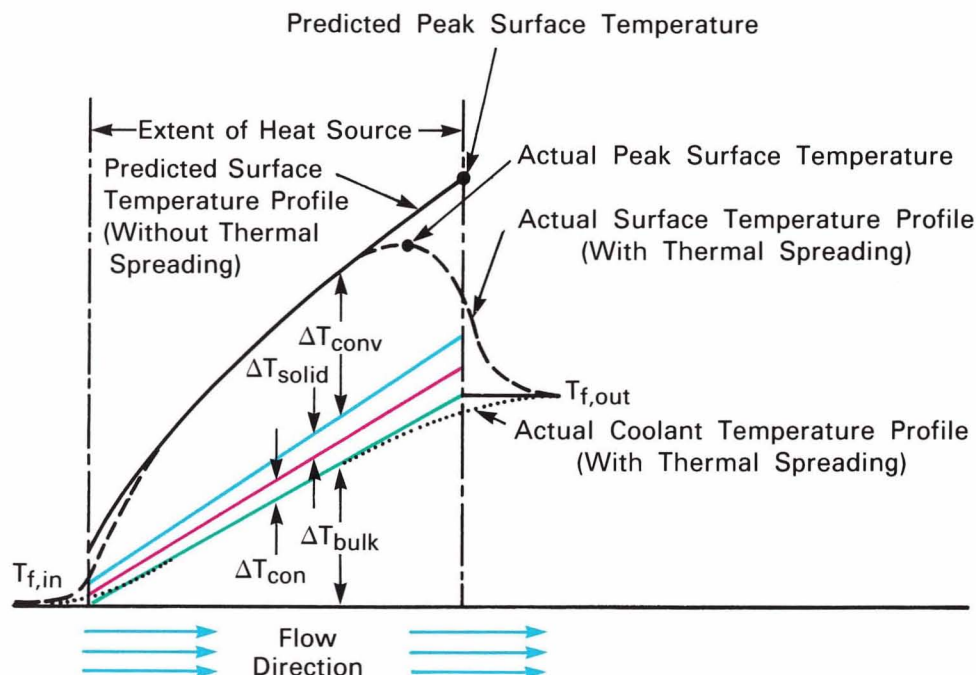

Fig. 6 — *Various thermal resistance components, the greatest being R''_{bulk} and R''_{conv}, contribute to the temperature variations in the streamwise direction within a heat sink.*
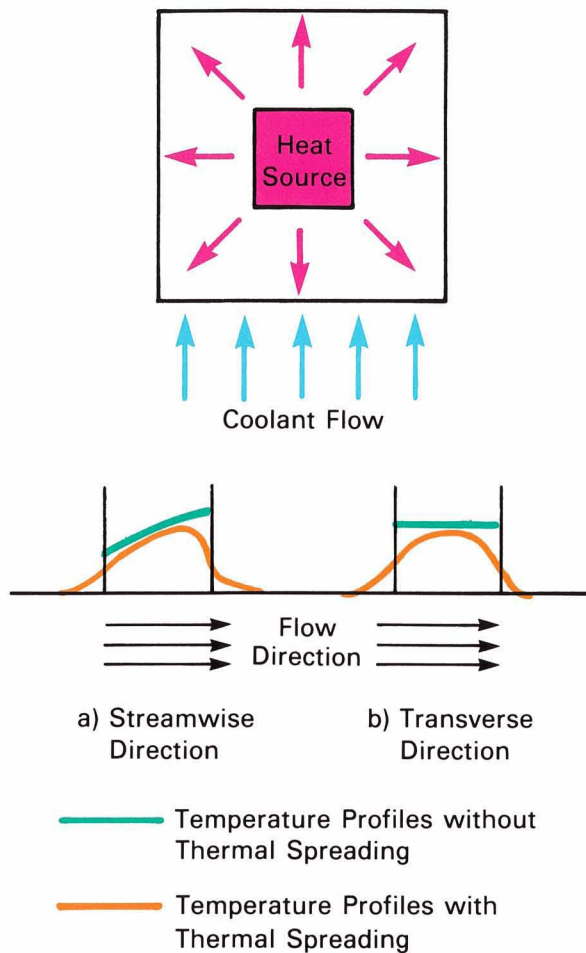
Fig. 7 — *Effect of thermal spreading at the heat-source perimeter.*

Figures 8 and 9 show thermal resistance and pumping power per unit area as functions of channel width. (See Refs. 5 and 11 for additional performance prediction comparisons.) The results for a reference-case heat-sink design are given by the three solid curves in Fig. 8. (R''_{solid} and R''_{con} are not shown because they are small and vary little with channel width.) These curves show that R''_{bulk} decreases with increasing channel width because more coolant can be forced through a channel with a larger equivalent diameter, for a given overall pressure drop. R''_{conv} increases for laminar flow; it is somewhat smaller for turbulent flow. Total thermal resistance is dominated by R''_{bulk} for small channel widths and by R''_{conv} for moderate to large channel widths. The results show that a microchannel heat sink can have

an R''_{tot} smaller than $0.1°C/(W/cm^2)$. The required pumping power per unit surface area is less than $10 W/cm^2$.

The blue and red curves in Fig. 8 show the effect on the heat-sink performance of changing the channel length. The thermal performance of the shorter channel design is superior, but this performance is obtained at the expense of a large increase in the pumping-power requirement. The thermal performance of the longer channel design is not quite as good, but the coolant distribution system to and from the heat sink is considerably simpler.

If a heat sink is made of copper, the total thermal resistance decreases — the thermal conductivity of copper is 2.7 times that of silicon (red curves in Fig. 9). To improve heat-sink performance, a heat sink and an IC can be fabricated independently and then bonded via a low-thermal-resistance interface (such as a micro-capillary interface). The copper microchannel heat sink can provide better thermal performance than a heat sink directly fabricated within the IC itself.

The orange curves in Fig. 9 show the effect of using Freon (CCl_2F_2) as the liquid coolant, rather than water. Because of its low reactivity, Freon is commonly used in direct-contact pool boiling cooling for electronics. The thermal performance of Freon is not quite as good as the thermal performance of water, but the pumping power requirements are similar.

The blue curves in Fig. 9 show the result for constant pumping power per unit heater-surface area, P''; the green curves show the result for constant coolant volumetric flow rate per unit of heater surface, V''. For fixed pumping power, the optimal laminar flow design occurs at $W_c \approx 50$ μm. For the fixed flow-rate constraint, the thermal resistance increases and the pumping power decreases with channel width. As expected, the constraints predict identical performance for $P'' = \Delta P \cdot V''$.

FABRICATION

Large arrays of surface-emitting GaInAsP/InP laser diodes [12] can dissipate several hundred W/cm^2. To address this cooling challenge, microchannel heat sinks were fabricated in InP, the
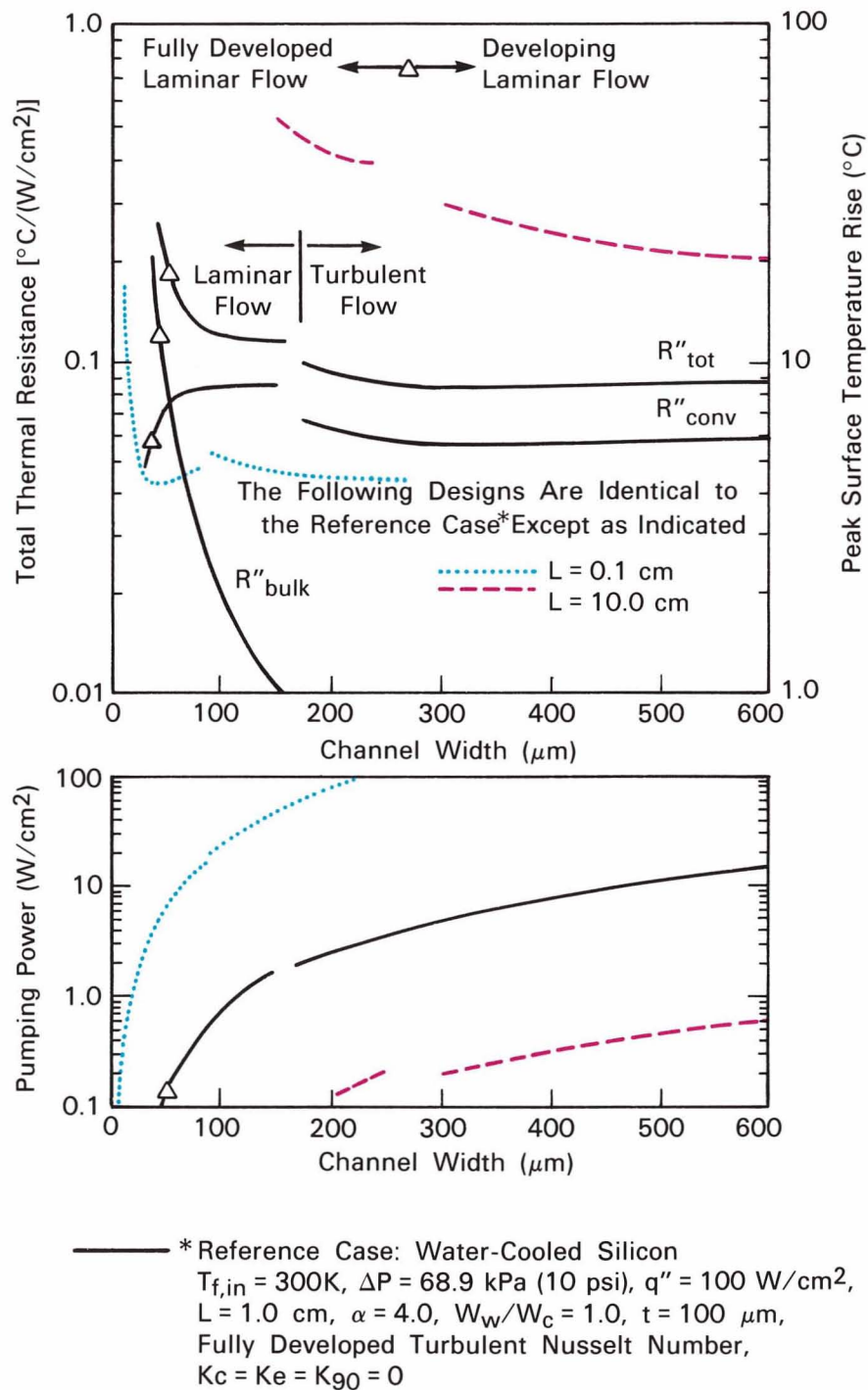
Fig. 8 — *Total thermal resistance and pumping power requirements are shown as functions of channel width. The pressure drop is held constant for these curves.*
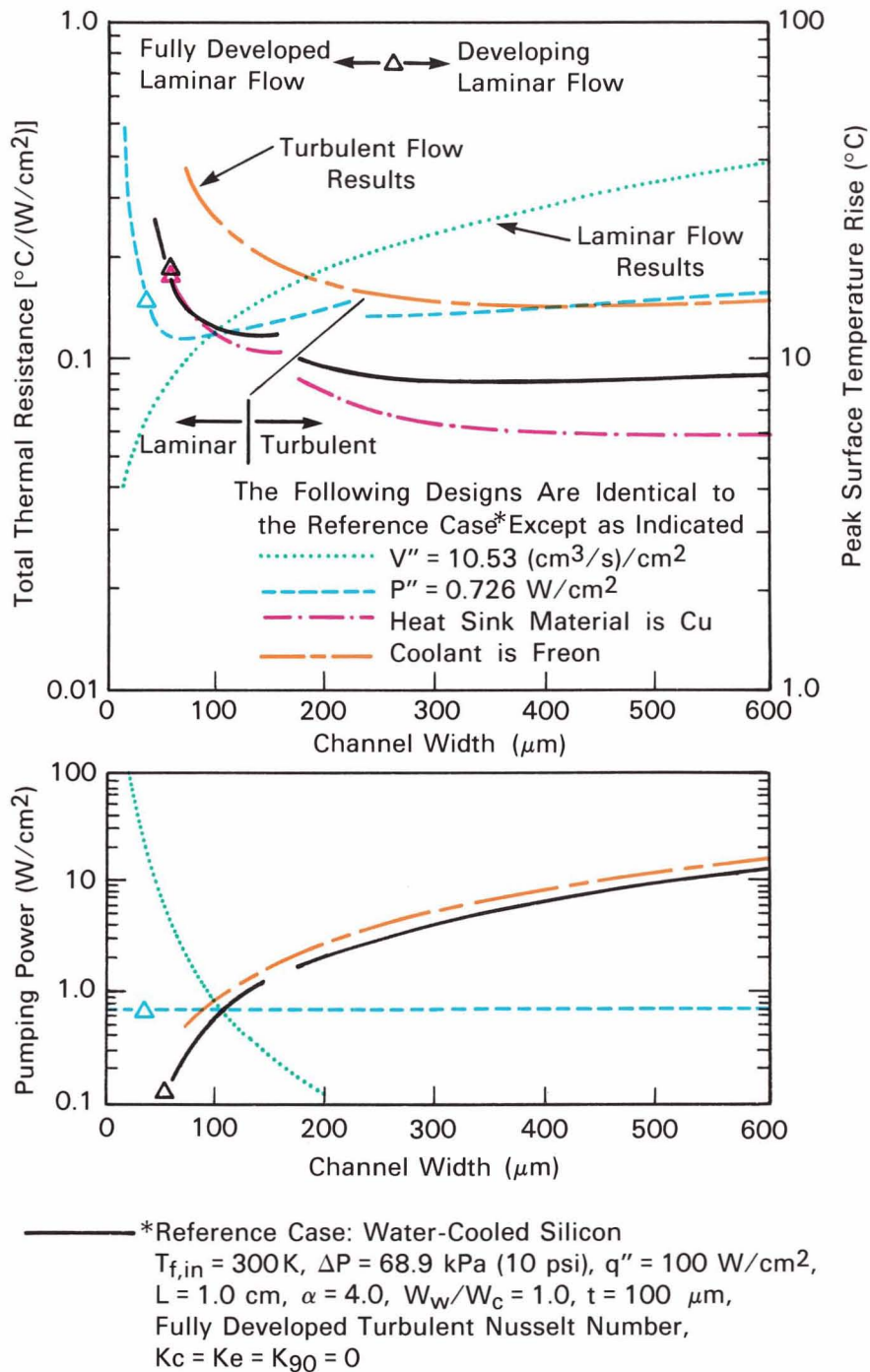
Fully Developed Laminar Flow ← △ → Developing Laminar Flow

Turbulent Flow Results

Laminar Flow Results

Laminar | Turbulent

The Following Designs Are Identical to the Reference Case*Except as Indicated

······· V″ = 10.53 (cm³/s)/cm²
– – – P″ = 0.726 W/cm²
–·–·– Heat Sink Material is Cu
– – – Coolant is Freon

*Reference Case: Water-Cooled Silicon
$T_{f,in}$ = 300 K, ΔP = 68.9 kPa (10 psi), q″ = 100 W/cm²,
L = 1.0 cm, α = 4.0, W_w/W_c = 1.0, t = 100 μm,
Fully Developed Turbulent Nusselt Number,
$K_c = K_e = K_{90} = 0$

Fig. 9 — *Total thermal resistance and pumping power requirements are shown for various coolants, heat-sink materials, and coolant flow-rate constraints.*

substrate material of these laser diodes. Other researchers have produced microchannels in Si, but this is the first demonstration of microchannel heat sinks in InP. A method was also developed to fabricate microchannels in aluminum.

Two methods have been used to fabricate microchannels: precision sawing and orientation-dependent etching. Precision sawing with semiconductor dicing saws is an efficient production technique for Si. However, because of its brittleness, sawing does not work well with InP [5]; an InP heat sink's fins frequently chip and break.

Unlike sawing, orientation-dependent etching works well in forming microchannels in InP [5] and in Si [1,2,4]. Microchannels were etched along the <011> direction in InP, using a 3:1 mixture (by volume) of H_3PO_4:HCl at room temperature. The channels were patterned in a 3,000-Å layer of phosphosilicate glass (PSG), applied to a polished chip surface that was preetched with full-strength potassium ferricyanide. (Pre-etch is required for good adhesion of the PSG. Without the pre-etch, undesirable undercutting occurs.) The channel depth etching rate averaged 0.62 μm/min, and the undercutting etching rate averaged 0.22 μm/min.

Figure 10 shows three views of InP microchannel heat sinks. The top view illustrates that the channels do not extend to the edge of the chip, which eliminates the need to seal the channel ends. The channel-end shape is shown in a streamwise view; the angle of the solid material is 35° to 38°. This angle helps deflect the inlet and outlet coolant flow and therefore helps reduce the pressure drop.

The wavy appearance of the fin tips in the top view is due to drooping of the PSG mask (caused by undercutting). This waviness produces roughness features in the channel walls, which propagate to the fin base as the 35° to 38° triangular shapes seen in the streamwise view. This roughness can serve as a turbulence promoter. Increased turbulence increases heat transfer rates at the expense of increasing pumping power requirements. The channel bottoms in the top view have a "granular" texture. This

texture is due to small mounds created by defects. These defects are in the polished surface before etching starts. The mounds also have 35° to 38° edges.

The transverse view in Fig. 10 shows that the channel and fin cross-sections are quite uniform. When the PSG mask adheres properly, the channel uniformity is generally within 5%. Channel uniformity of 5% or better is recommended because thermal performance (for the same pumping power) decreases exponentially with increasing nonuniformity [13].

As an alternative to forming microchannels in InP chips, fabrication techniques were developed for cold plate microchannel heat sinks. A numerical-control milling machine was used to cut microchannels in aluminum [5]. An arbor was constructed with five 250-μm (thickness) × 3.175-cm (diameter) circular jewelers' saws, each separated by 240-μm shim-stock. A milling rate of 1.25 cm/min produced heat sinks at a rate of approximately 20 cm^2/h.

Increasing the number of saws will provide the production rates necessary for mass production and commercialization. Other fabrication methods, including extrusion and laser machining, may also be suitable for mass production.

EXPERIMENTS

Thermal and fluid performance tests have been conducted on microchannel heat sinks fabricated directly within InP substrates. The three-sided etched-channel chips were packaged to provide coolant flow to and from the chip, as shown in Fig. 11. A cover plate with inlet and outlet manifold slots was epoxied to the chip. The cover plate is Corning #7059 glass, which has a coefficient of thermal expansion that closely matches the coefficient of InP. Trabond F-113 epoxy, which wets InP surfaces well (ensuring strong bonds), was used to bond the chip to the cover plate. The epoxy has good stability at the chip operating temperatures for periods in the tens of hours. (No long-term tests have been conducted to date.) Devcon five-minute epoxy was used to attach the cover plate to the Lexan coolant-manifold block.
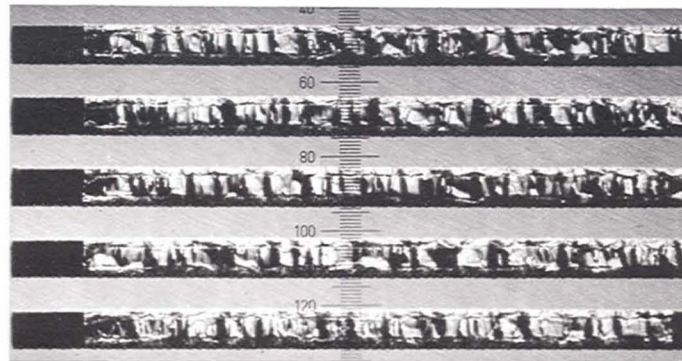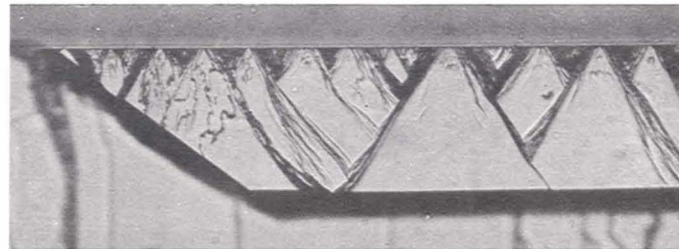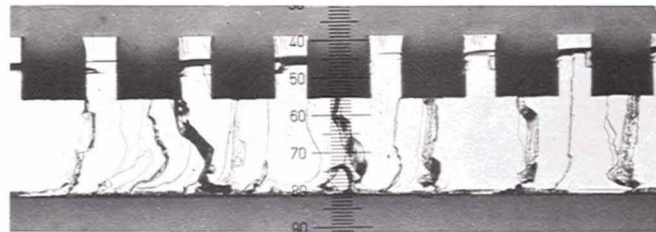
42

a) Top View (~210-μm-Wide Channels on 375-μm Centers).

b) Streamwise View (b ~ 160-μm).

c) Transverse View (~160-μm-Wide Channels on 250-μm Centers, α ~ 1.0).

Fig. 10 — *Orientation-dependent etching produced these InP microchannels.*

The resistor heat-source design that provided the thermal load for the heat-sink tests is shown in Fig. 12. Four 0.25 × 0.25-cm square resistors were fabricated directly into the top surface of the test chips. The resistance was typically 16 to 19 Ω/square; the resistance uniformity among the four resistors was better than ±1.1%. Each resistor received power independently of the other resistors, which allowed investigation of thermal spreading at each heat-source perimeter.

The fluid performance of a typical microchannel heat sink is shown in Fig. 13. In this figure, the pressure drop is plotted as a function of Reynolds number. The uncertainty in the Reynolds number is primarily due to uncertainty in the channel equivalent diameter. The uncertainty in the pressure drop is approximately equal to the size of the data points. The predicted pressure drop agrees, within 5% to 10%, with the experimental data for laminar flow. (Roughness does not seriously affect the apparent friction factor in laminar flow.) The turbulent flow pressure drop predictions, however, are low because those predictions assumed that the channel surfaces were smooth. The apparent friction factor is larger than it is for smooth surfaces because the roughness features extend past the turbulent-flow laminar sublayer.

The thermal performance of a microchannel heat sink fabricated in Si is shown in Fig. 14.
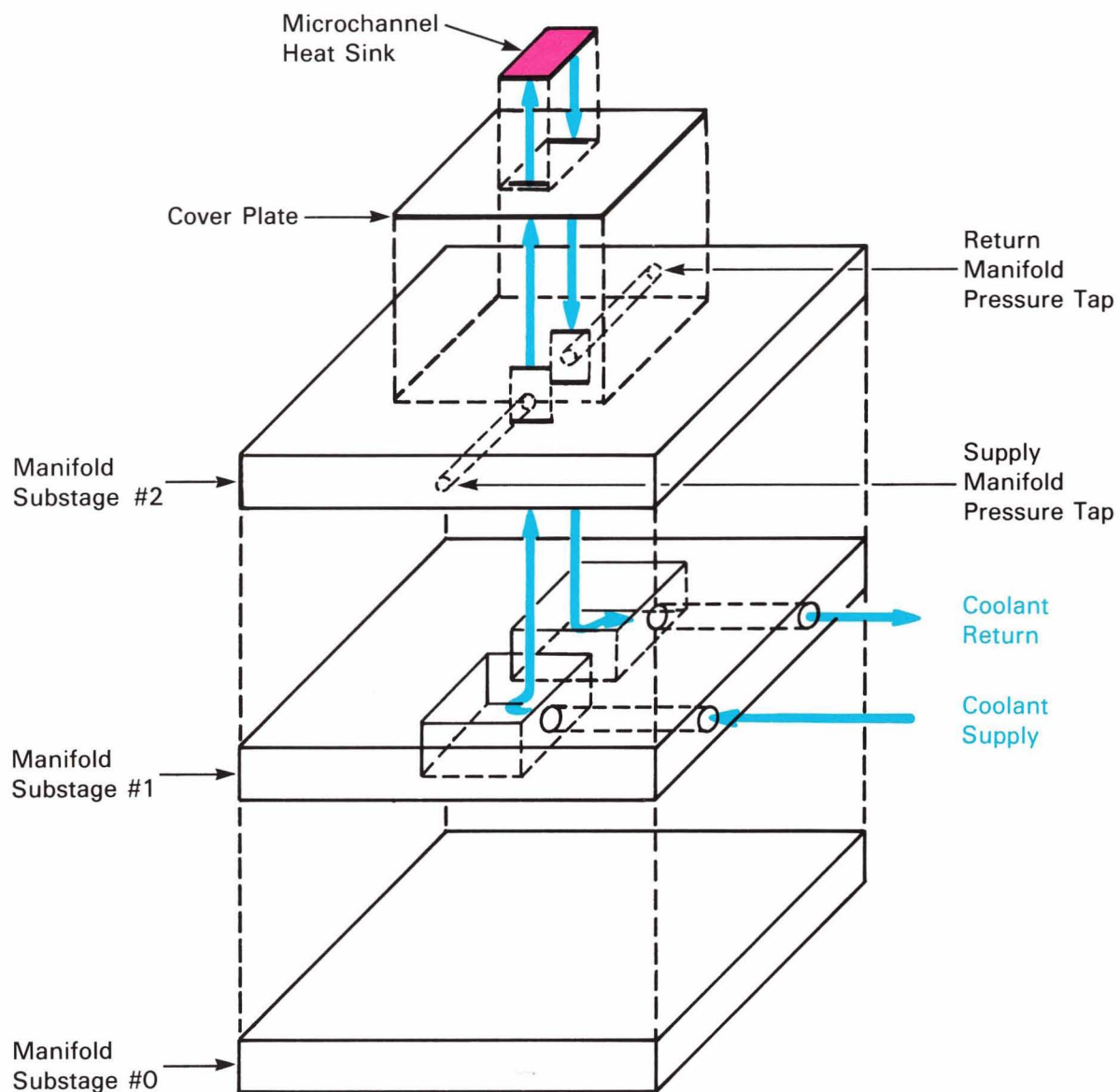
Fig. 11 — This coolant-distribution manifold supplies coolant to microchannel heat sinks during thermal tests.

The thermal performance predicted using the theory in this article is presented for comparison. Because the heat source is large, thermal spreading does not seriously affect the thermal performance.

InP microchannel heat sinks were tested at heat dissipation rates as high as 1,056 W/cm^2 with thermal resistance as low as 0.072°C/(W/cm^2). A contour map of typical surface temperature profiles for microchannel-cooled InP chips is shown in Fig. 15a. This figure shows how thermal spreading affects the thermal performance of a heat sink. Thermal spreading influences thermal performance because, in this case, the thermal-spreading diffusion length is comparable to the size of the resistor heat sources. Figure 15b compares theory and experiment — the predicted total thermal resistance is approximately 20% larger than the experimental result. This discrepancy is thought to be the result of the use of two superimposed, one-dimensional thermal-spreading models to
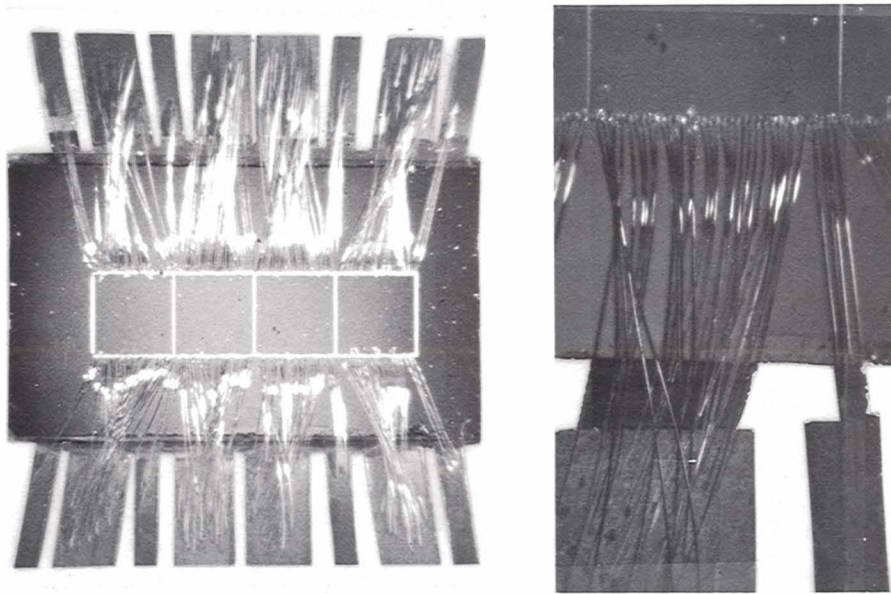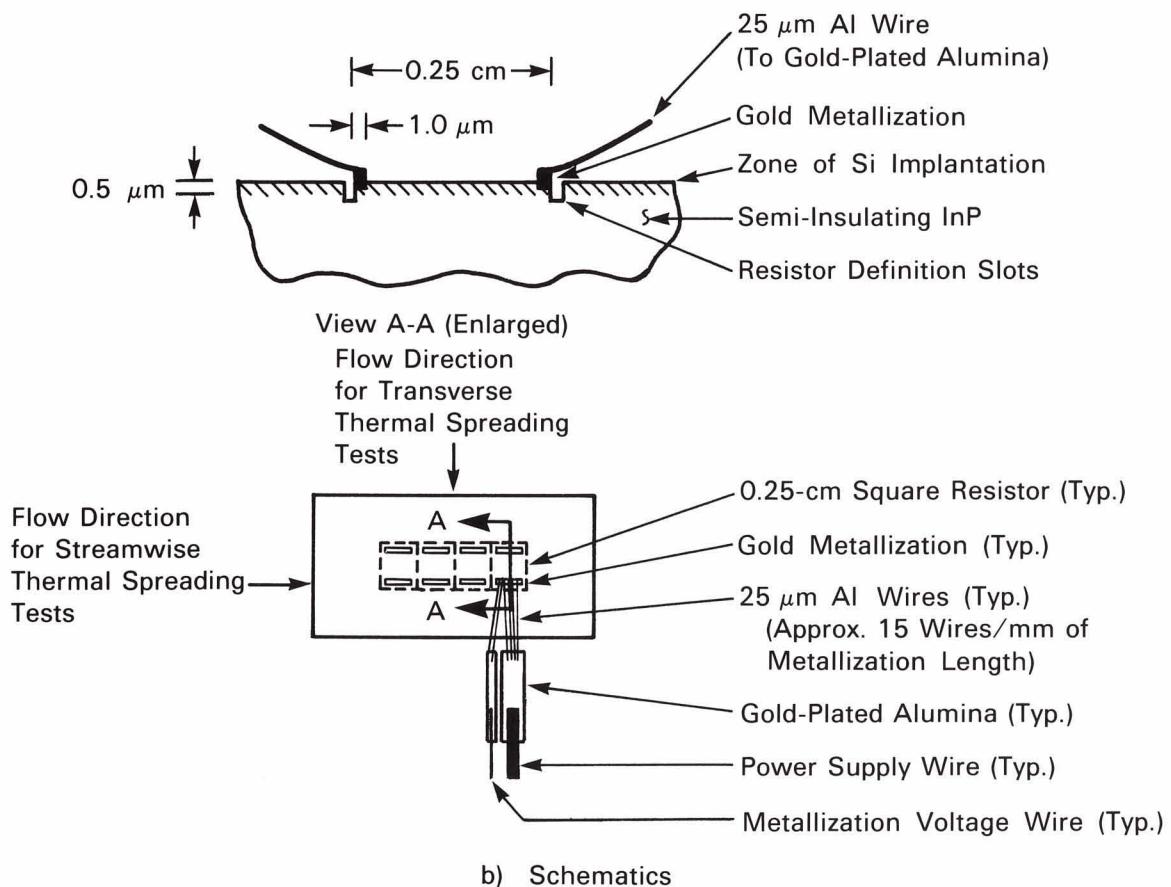
a)   Photographs of a Typical Test Chip

b)   Schematics

Fig. 12 — These test-chip resistors provided thermal loads to heat sinks to measure the heat sinks' dissipation capability.

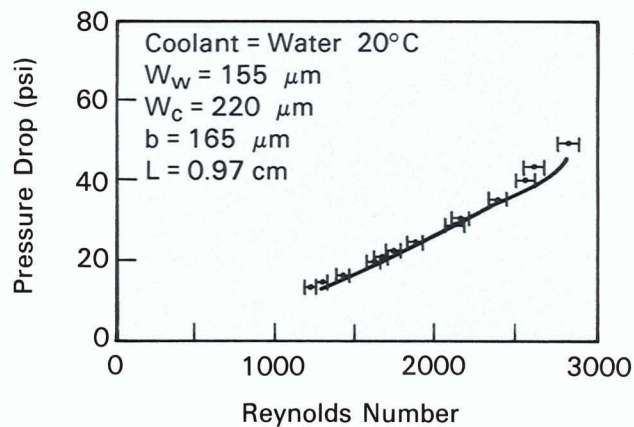*Fig. 13 — Predicted and experimental values of pressure drop are plotted as functions of Reynolds number.*

Theoretical Values

Experimental Data Points Obtained from Ref. 4

$V'' = 1.277$ $(cm^3/s)/cm^2$
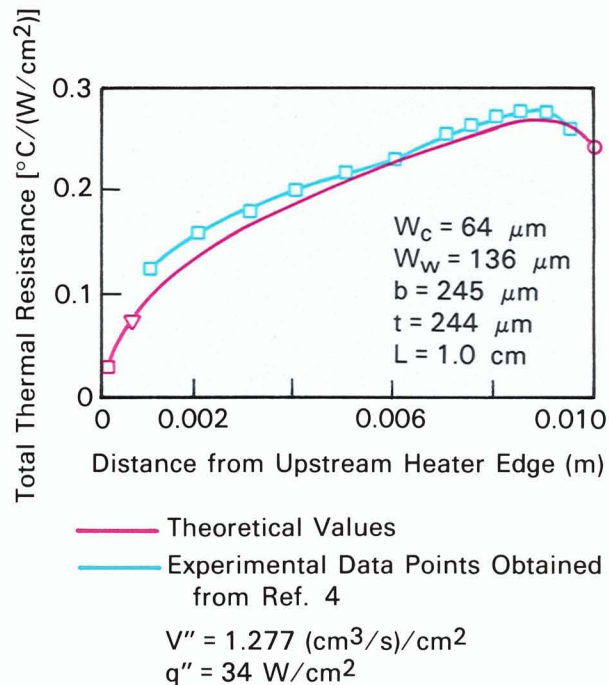
$q'' = 34$ W/cm^2

Fig. 14 — The local thermal resistance of a water-cooled Si microchannel heat sink increases with increasing distance from the upstream heater edge.

predict lateral thermal spreading at the heat-source perimeter, instead of a detailed two-dimensional model [5].

Table 2 lists experimental results reported by several researchers who have studied microchannel heat sinks. The relative performance of the heat-sink designs is difficult to rank,

Table 2 — Experimental Performance Parameters

Ref.	Heater Size (cm × cm)	W_w (μm)	W_c (μm)	b (μm)	L (cm)
[14]	0.508	127	127	12,700	0.635
[15]	0.7	2,540	5,870	1,000	5.0 (est.)
[16]	0.8	2,540	800	400	8.3 (est.)
[17]	0.8	340	340	900	2.4
[4][a]	1.0	35	55	400	2.00 (overall)
[5]	0.25	155	220	165	0.97
[19]	3.8	100	200	1,700	5.0

Ref.	Coolant	Pressure Drop (kPa)	Flow Rate $(cm^3/s)/cm^2$	Thermal Resistance $[°C/(W/cm^2)]$
[14]	Air	1.2	1,940	0.88
[15]	Water	110	7.9	0.17
[16]	Water	20	0.21	2.1
[17]	Water	20	—	0.32
[4]	Water	365	4.73	0.083
[5]	Water	267	11.3	0.072
[19]	Water	—	4.4	0.29
	Air	—	88.9	10.1

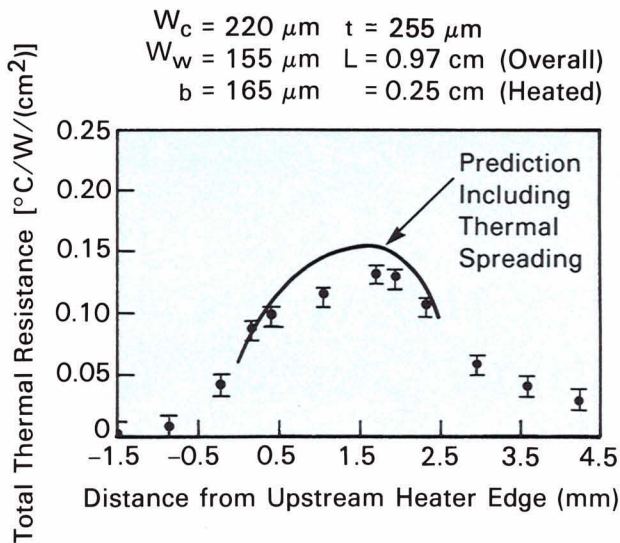[a] 35-μm (length) interrupted cooling fins as opposed to continuous fins.

because it depends on the applications for which the heat sinks were designed. For example, some heat sinks were designed as multichip modules [15-17], which do not perform quite as well as single-chip modules [4,5]. Part of the performance advantage of single-chip modules comes from fabricating microchannels directly within a chip. The channels of multichip modules, in contrast, are fabricated in a cold plate to which the chips are attached.

CONCLUSIONS

Microchannel heat sinks dissipate large amounts of heat with relatively little surface temperature rise. These heat sinks are useful for a wide variety of applications, including microelectronics, diode laser arrays, and high-energy-laser mirrors. The thermal performance of microchannel heat sinks is approximately two orders of magnitude better than the thermal performance of other devices currently used to cool microelectronic devices. Furthermore, the pumping power required to force

Flow Direction

$q'' = 170.9 \text{ W/cm}^2$
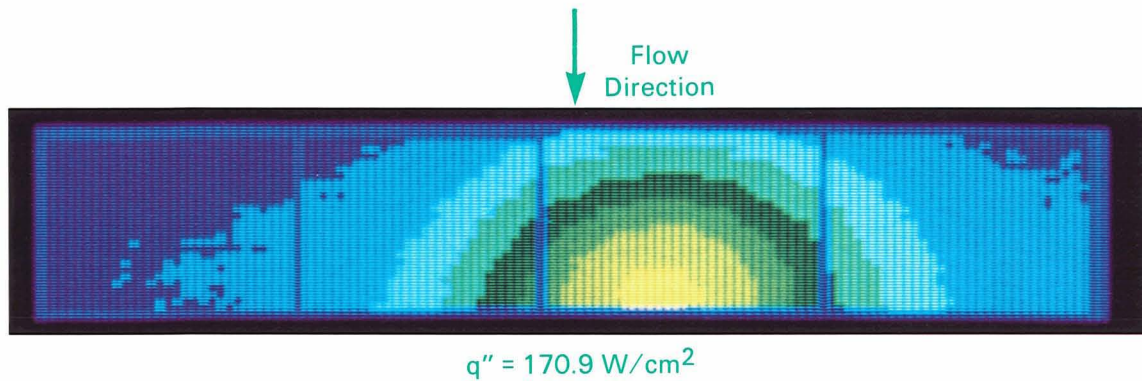
a) Surface Temperature Contours for
One Heater Energized

$W_c = 220 \ \mu m$ $t = 255 \ \mu m$
$W_w = 155 \ \mu m$ $L = 0.97$ cm (Overall)
$b = 165 \ \mu m$ $= 0.25$ cm (Heated)

b) Comparison Between Data and Theory [5]

Fig. 15 — a) The effects of thermal spreading are shown by the contours in this photograph. One heater is operating; the other three are off. b) Predicted and experimental values of total thermal resistance are plotted as functions of distance from the upstream heater edge.

liquid coolants through these heat sinks can be kept to less than 10 W/cm².

By using orientation-dependent acid etching, microchannel heat sinks can be fabricated in <100> InP. The thermal performance of InP microchannel heat sinks is excellent — thermal resistance as low as $0.072°C/(W/cm^2)$ and heat dissipation as high as 1,056 W/cm² have been measured for InP heat sinks. Fabrication techniques have also been developed for mass production of microchannel heat sinks in aluminum and other metals.

REFERENCES

1. D.B. Tuckerman and R.F.W. Pease, "High-Performance Heat Sinking for VLSI," *IEEE Electron Device Lett.* **EDL-2,** 126 (1981).
2. D.B. Tuckerman and R.F.W. Pease, "Ultrahigh Thermal Conductance Microstructures for Cooling Integrated Circuits," *Proc. 32nd Electronics Components Conf.,* p. 145 (1981).
3. D.B. Tuckerman and R.F.W. Pease, "Optimized Convective Cooling Using Micromachined Structures," *Electrochemical Soc. Extended Abstracts* **82,** 197 (1982).
4. D. B. Tuckerman, "Heat-Transfer Microstructures for Integrated Circuits," *PhD Thesis,* Stanford University, Stanford, CA (1984).
5. R.J. Phillips, "Forced-Convection, Liquid-Cooled, Microchannel Heat Sinks," *Masters Thesis,* Massachusetts Institute of Technology, Cambridge, MA (1987).
6. V. Gnielinski, "New Equations for Heat and Mass Transfer in Turbulent Pipe and Channel Flow," *Int. Chem. Eng.* **84,** 82 (1962).
7. J.P. Holman, *Heat Transfer,* McGraw-Hill, New York (1976).
8. R. C. Joy and E.S. Schlig, "Thermal Properties of Very Fast Transistors," *IEEE Trans. Electron Devices* **ED-17,** 586 (1970).
9. D.B. Tuckerman and R.F.W. Pease, "Microcapillary Thermal Interface Technology for VLSI Packaging," *Symp. on VLSI Technology, Digest,* p. 60 (1983).
10. A.D Kraus and A. Bar-Cohen, "Thermal Analysis and Control of Electronic Equipment," McGraw-Hill, New York (1983).
11. R.J. Phillips, L.R. Glickman, and R. Larson, "Forced-Convection, Liquid-Cooled, Microchannel Heat Sinks for High-Power-Density Microelectronics," *Proc. of the Int. Symp. on Cooling Technology for Electronic Equipment,* Pacific Institute for Thermal Engineering, Honolulu, HI (1987).
12. Z.L. Liau and J.N. Walpole, "Surface Emitting GaInAsP/InP Laser With Low Threshold Current and High Efficiency," *Appl. Phys. Lett.* **46,** 115 (1985).

Symbols

a	Heat source characteristic dimension [m]		R''_{int}	Interface thermal resistance [°C/(W/cm²)]
b	Channel height [m]		R''_{solid}	Solid material thermal resistance [°C/(W/cm²)]
C_{pf}	Coolant specific heat [J/kg-°C]		R''_{spread}	Spreading thermal resistance [°C/(W/cm²)]
De	Channel equivalent diameter [m]			
f_{app}	Apparent friction factor		R''_{tot}	Total thermal resistance [°C/(W/cm²)]
g_c	Units constant [kg-m/N-s]			
h	Convective heat transfer coefficient [W/m²-°C]		Re	Reynolds number
			t	Solid material thickness [m]
J	Mechanical equivalent of heat [N-m/J]		V	Average coolant velocity [m/s]
k_f	Coolant thermal conductivity [W/m-°C]		V''	Coolant volumetric flow rate per unit surface area [(cm³/s)/cm²]
k_w	Heat-sink material thermal conductivity [W/m-°C]		W_c	Channel width [m]
			W_w	Fin width [m]
L	Channel length [m]		x	Distance from channel entrance [m]
m	Fin efficiency parameter [m⁻¹]		η_f	Fin efficiency
Nu	Nusselt number		α	Channel aspect ratio
P''	Pumping power per unit surface area [W/cm²]		ΔP	Coolant pressure drop [N/m²]
Pr	Coolant Prandtl number		ΔT	Wall-to-coolant temperature difference [°C]
q''	Heat transfer rate per unit area [W/m²]		ΔT_{surf}	Peak surface temperature rise above inlet coolant temperature [°C]
Q	Total heating rate [W]		ΔT_{tot}	Total temperature rise [°C]
R''_{bulk}	Coolant bulk temperature rise thermal resistance [°C/(W/cm²)]		ΔT_{visc}	Viscous heating coolant temperature rise [°C]
R''_{con}	Contraction thermal resistance [°C/(W/cm²)]		ν_f	Coolant kinematic viscosity [m²/s]
			ρ_f	Coolant density [kg/m³]
R''_{conv}	Convective thermal resistance [°C/(W/cm²)]			

13. R.K. Shah and A.L. London, "Effects of Nonuniform Passages on Compact Heat Exchanger Performance," *J. Eng. Power* **102,** 653 (1980).
14. N. Goldberg, "Narrow Channel Forced Air Heat Sink," *IEEE Trans. Components Hybrids Manuf. Technol.* **CHMT-7,** 154 (1984).
15. D. Nayak, L.T. Hwang, I. Turlik, and A. Reisman, "A High-Performance Thermal Module for Computer Packaging," *J. Electron. Mater.* **16**, 357 (1987).
16. T. Kishimoto and T. Ohsaki, "VLSI Packaging Technique Using Liquid-Cooled Channels," *Proc. 1986 IEEE Electronic Component Conf.*, p. 595 (1986).
17. S. Sasaki and T. Kishimoto, "Optimal Structure for Microgrooved Cooling Fin for High-Power LSI Devices," *Electron Lett.* **22**, 1332 (1986).
18. A. Bar-Cohen, "Thermal Management of Air- and Liquid-Cooled Multi-chip Modules," *IEEE Trans. Components Hybrids Manuf. Technol.* **CHMT-10,** 159 (1987).
19. M. Mahalingam, "Thermal Management in Semiconductor Device Packaging," *Proc. IEEE* **73**, 1396 (1985).

ACKNOWLEDGMENTS
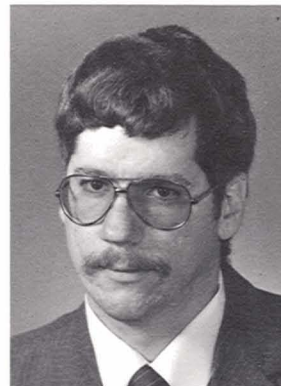
RICHARD J. PHILLIPS has worked for Lincoln Laboratory since 1983. A member of the Optical Systems Engineering Group, he studies beam-path conditioning systems for high-energy laser systems. Rick received a bachelor's degree in mechanical engineering from Colorado State University in 1982 and a master's degree in mechanical engineering from MIT in 1987. His varied leisure time activities include canoeing, fishing, scuba diving, and travel.